AGU PUBLICATIONS

Geophysical Research Letters

RESEARCH LETTER
10.1002/2015GL064968

Special Section:
First Results from the MAVEN Mission to Mars

Low-frequency waves in the Martian magnetosphere and their response to upstream solar wind driving conditions

Suranga Ruhunusiri[1], J. S. Halekas[1], J. E. P. Connerney[2], J. R. Espley[2], J. P. McFadden[3], D. E. Larson[3], D. L. Mitchell[3], C. Mazelle[4,5], and B. M. Jakosky[6]

[1]Department of Physics and Astronomy, The University of Iowa, Iowa City, Iowa, USA, [2]NASA Goddard Space Flight Center, Greenbelt, Maryland, USA, [3]Space Sciences Laboratory, University of California, Berkeley, California, USA, [4]IRAP, CNRS, Toulouse, France, [5]Paul Sabatier University, Toulouse, France, [6]Laboratory for Atmospheric and Space Physics, University of Colorado Boulder, Boulder, Colorado, USA

Abstract We characterize low-frequency plasma waves in the Martian magnetosphere and in the upstream region by using transport ratios. To compute the transport ratios, we use Mars Atmosphere and Volatile EvolutioN mission's (MAVEN) solar wind ion analyzer and suprathermal and thermal ion composition instrument measurements of the ion moments and the magnetometer measurements of the magnetic field. We find that the Alfvén waves are the most dominant wave mode in the upstream region and the magnetosheath. Fast waves are found frequently near the bow shock and the magnetic pileup boundary. Mirror and slow waves, on the other hand, occur much less frequently. We also find that the Alfvén and fast wave occurrences vary dominantly near the bow shock in response to the solar wind dynamic pressure.

Key Points:
- Transport ratios are used for characterization of low-frequency plasma waves at Mars
- Alfvén and fast waves have the highest occurrence ratios in the Martian magnetosphere
- Waves near the bow shock exhibit occurrence variability in response to solar wind dynamic pressure

Correspondence to:
S. Ruhunusiri,
suranga-ruhunusiri@uiowa.edu

Citation:
Ruhunusiri, S., J. S. Halekas, J. E. P. Connerney, J. R. Espley, J. P. McFadden, D. E. Larson, D. L. Mitchell, C. Mazelle, and B. M. Jakosky (2015), Low-frequency waves in the Martian magnetosphere and their response to upstream solar wind driving conditions, *Geophys. Res. Lett.*, *42*, doi:10.1002/2015GL064968.

Received 17 JUN 2015
Accepted 18 JUL 2015

1. Introduction

The interaction of the solar wind with planetary magnetospheres leads to excitation of plasma waves in the upstream region and within the magnetosphere. While Mars does not have an intrinsic magnetic field, it has an induced magnetosphere resulting from the interaction of the solar wind with its ionosphere. Furthermore, the weaker gravity of Mars means that it has an extended exosphere which spreads beyond the planetary bow shock. Thus, the solar wind directly interacts not only with the induced magnetosphere of Mars but also with its exosphere generating plasma waves which often have the highest power near and below the local gyrofrequency, i.e., low-frequency (LF) plasma waves. The simultaneous existence of the induced magnetosphere and the extended exosphere at Mars presents us a unique environment to study these low-frequency plasma waves in the solar system.

Studying these waves is of interest because they can play an important role in the momentum and energy transfer in the Martian magnetosphere. Moreover, these waves are an indirect way to infer the underlying physics operating in various regions of the Martian magnetosphere. For example, ion cyclotron-like waves are generated when the solar wind interacts with the pickup ions from the exosphere [*Russell et al.*, 1990] or reflected ions from the bow shock [*Gary*, 1991]. Mirror mode waves, on the other hand, indicate the presence of local temperature or pressure anisotropy [*Bertucci et al.*, 2004]. Low-frequency plasma waves may also play a significant role in the atmospheric loss at Mars [*Ergun et al.*, 2006; *Lundin et al.*, 2011].

Previous characterizations of low-frequency waves at Mars were mainly performed using measurements of either the magnetic field or electron and ion density [*Russell et al.*, 1990, 1992; *Brain et al.*, 2002; *Mazelle et al.*, 2004; *Wei and Russell*, 2006; *Romanelli et al.*, 2013; *Espley et al.*, 2004; *Espley*, 2005; *Bertucci et al.*, 2013; *Winningham et al.*, 2006; *Gunell et al.*, 2008; *Lundin et al.*, 2011]. Using the Phobos-2 magnetometer *Russell et al.* [1990] observed waves at the proton gyrofrequency upstream of Mars and interpreted them as arising from pickup protons from the Martian exosphere. *Espley et al.* [2004] and *Espley* [2005], using the Mars Global Surveyor (MGS) magnetometer measurements, identified the dayside magnetosheath oscillations as mirror mode waves and the nightside oscillations as ion cyclotron instabilities. *Gurnett et al.* [2010] observed large electron density and magnetic field fluctuations in the Martian ionosphere with the aid of Mars Advanced Radar for Subsurface and Ionosphere Sounding (MARSIS) instrument aboard Mars Express, and they suggested several possible sources for these waves including Kelvin-Helmholtz instability.

Table 1. Value Ranges for the Transport Ratios for Identification of the LF Wave Modes in a High Beta Plasma Based on *Song et al*. [1994][a]

Wave Mode	$T_R = \frac{\left(\delta\mathbf{B}\cdot\delta\mathbf{B}-\delta B_{\parallel}^2\right)}{\delta B_{\parallel}^2}$	$C_R = \frac{\delta N_i^2}{N_{i0}^2} / \frac{\delta\mathbf{B}\cdot\delta\mathbf{B}}{B_0^2}$	$P_R = \frac{\delta N_i}{N_{i0}} / \frac{\delta B_{\parallel}}{B_0}$	$D_R = \frac{\delta\mathbf{V}_i\cdot\delta\mathbf{V}_i}{V_{i0}^2} / \frac{\delta\mathbf{B}\cdot\delta\mathbf{B}}{B_0^2}$
Alfvén and quasi-parallel slow	>1	<1	–	–
Quasi-parallel fast	>1	>1	–	–
Quasi-perpendicular fast	<1	–	>0	–
Quasi-perpendicular slow	<1	–	<0	>1
Mirror	<1	–	<0	<1

[a]Here $\delta B_{\parallel}$ is the fluctuating component of the magnetic field parallel to the ambient magnetic field.

In this investigation, we use both particle and field measurements to distinguish and characterize low-frequency plasma waves in the Martian magnetosphere and in the upstream region. In particular, we use ratios and phase differences among the fluctuations of the measured ion moments and magnetic fields to identify the waves. We use the MAVEN Solar Wind Ion Analyzer (SWIA) [*Halekas et al.*, 2013], Suprathermal and Thermal Ion Composition (STATIC) instrument [*McFadden et al.*, 2014], and the Magnetometer (MAG) [*Connerney et al.*, 2014] to obtain these measurements. SWIA and STATIC have higher data sampling rates than any of their predecessors at Mars. Specifically, SWIA and STATIC have cadences of 4 s that yields a Nyquist frequency of 0.13 Hz. This is often adequate to detect waves near and below the local gyrofrequency.

2. Low-Frequency Wave Identification

According to MHD theory, there are three normal modes for plasma waves with frequencies below the proton gyrofrequency: fast, Alfvén (intermediate), and slow. There is also a fourth mode, the mirror mode, and it requires temperature anisotropy for its generation. The primary difference between the mirror mode and the other three modes is that it has zero phase velocity in the plasma rest frame [*Song et al.*, 1994]. In the limit of the classical MHD, this fourth mode is also referred to as an entropy mode [*Song et al.*, 1994].

Two techniques are mainly used for identifying these four wave modes. In the first method, the wave's frequency and wavelength in the plasma rest frame are measured and they are compared with theoretical dispersion relations for the wave modes. However, this is not possible using a single spacecraft measurement because the frequency of the wave is often Doppler shifted due to the streaming solar wind. This Doppler shift can be corrected only if the wavelength is known. However, the wavelength measurement requires not one but two spacecraft.

The second technique is suitable for wave identification using measurements from a single spacecraft. This method requires calculation of transport ratios, which are correlation coefficients or ratios between the magnetic field fluctuations and particle moment fluctuations. *Gary* [1993] introduced this method of wave identification by computing transport ratios, and later, *Song et al.* [1994] and *Denton et al.* [1995] extended this method to identify low-frequency wave modes using only a handful of transport ratios. This method has been applied to identify waves in the Earth's magnetosheath and in the upstream region [*Song et al.*, 1994; *Denton et al.*, 1995; *Schwartz et al.*, 1996; *Hubert et al.*, 1998; *Blanco-Cano and Schwartz*, 1997].

3. Method

In this letter, we use the wave identification scheme developed by *Song et al.* [1994] for low-frequency wave identification. In this method, the four LF wave modes can be distinguished by using only four transport ratios: transverse ratio T_R, compressional ratio C_R, phase ratio P_R, and Doppler ratio D_R. These transport ratios are defined in Table 1, and their computation requires fluctuating components or Fourier components of the ion density δN_i, ion velocity $\delta\mathbf{V}_i$, magnetic field $\delta\mathbf{B}$, and mean values of the ion density N_{i0}, ion velocity V_{i0}, and the magnetic field B_0.

To compute the transport ratios, we first start with time series for SWIA measurements of the ion density and ion velocity, and MAG measurements of the magnetic field, Figures 1a–1c. Then, we Fourier transform these field and ion moments, for every 128 s interval. The sampling rate for the MAG instrument is 32 samples per second, much higher than that of SWIA. Thus, we take 4 s averages of the magnetic field prior to computing its

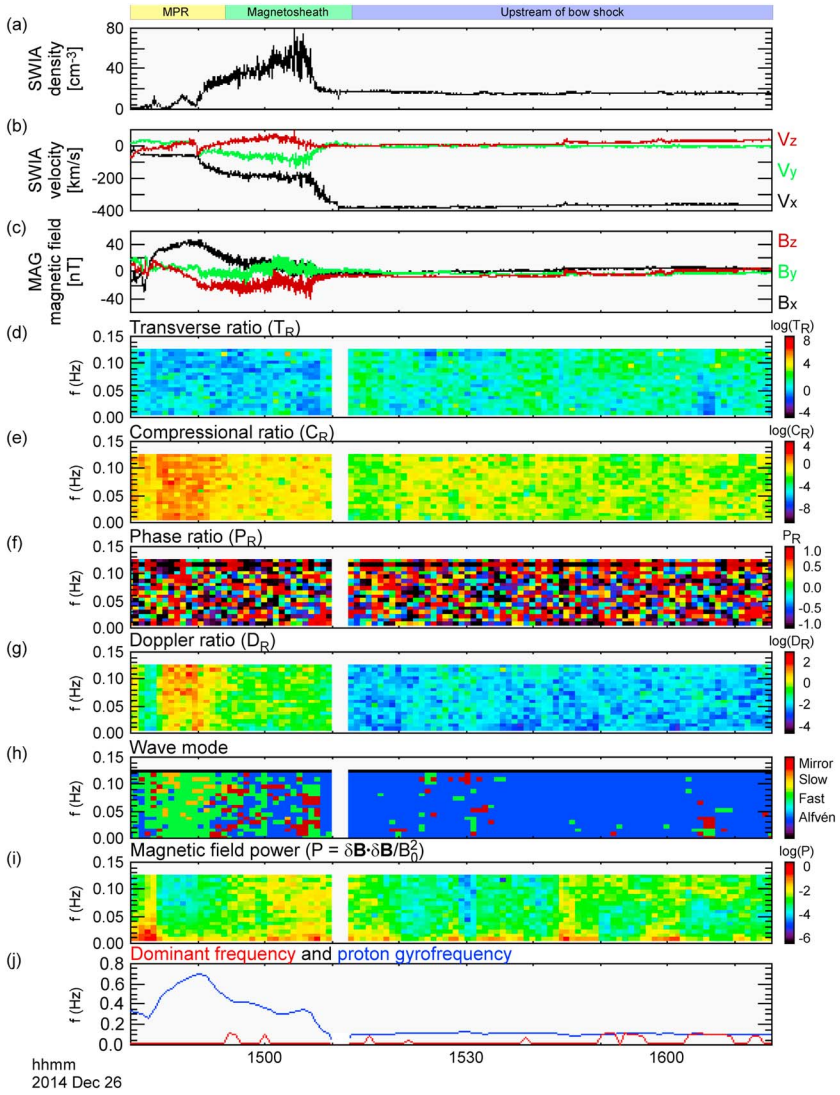

Figure 1. Time series of ion moments, magnetic field, and computed spectra of transport ratios and wave modes for a representative time segment when the spacecraft travels from the magnetic pileup region (MPR) to upstream of the bow shock. (a) SWIA ion density and (b) velocity along with the (c) MAG magnetic field are used to compute the spectra for (d–g) four transport ratios as defined in Table 1. These transport ratios are in turn used to identify the wave modes based on Table 1, yielding (h) a wave mode spectrum. (i) The magnetic field power spectrum is used to identify the wave modes corresponding to the highest power. (j) Frequency corresponding to the dominant power (dominant frequency) based on the magnetic field power spectrum is plotted along with the local proton gyrofrequency, computed from the magnetic field data.

Fourier transform. Finally, we compute the transport ratios for each frequency using the Fourier components of the ion density, velocity, and magnetic field and their mean values using the definitions in Table 1. This yields spectra of transport ratios, Figures 1d–1g.

Once the transport ratios are computed, a hierarchical scheme, shown in Figure 1 of *Song et al.* [1994] can be used to identify among the four wave modes based on the values for the transport ratios. For example, the wave mode is quasi-parallel fast if both the transverse and the compressional ratios are greater than one. We have tabulated the various ranges of the transport ratios used for the identification of the four LF wave modes in Table 1. In this wave mode identification method, the fast and slow waves are distinguished based on their propagation angle with respect to the ambient magnetic field, for example, as quasi-parallel versus quasi-perpendicular waves. This method can distinguish the four wave modes separately with the exception of Alfvén waves and the quasi-parallel slow waves.

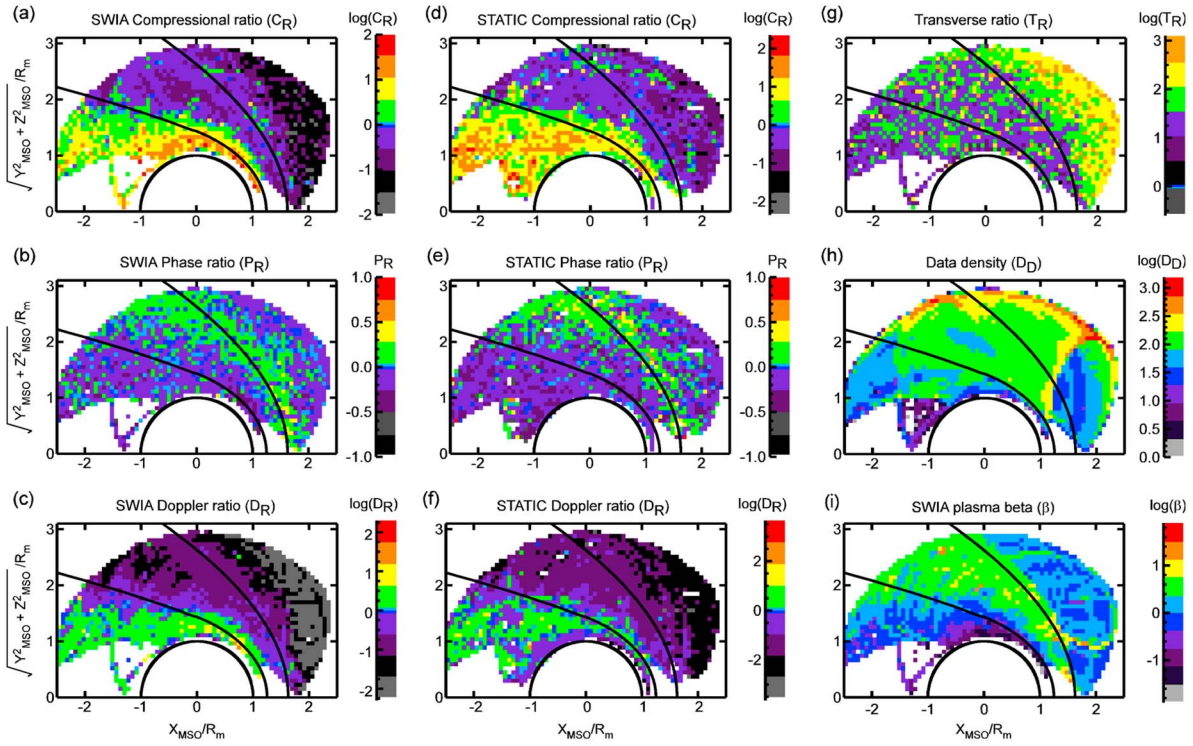

Figure 2. Orbit maps of the four transport ratios corresponding to the dominant wave modes. (a–c) Transport ratios based on MAG and SWIA measurements. (d–f) The transport ratios based on MAG and STATIC agrees with those based on SWIA. Thus, SWIA instrument limitations do not preclude us from inferring the qualitative and quantitative trends of these ratios downstream of the MPB. (g) Transverse ratio based on MAG measurements. The transport ratios show a wide variability when going from the upstream region to the magnetosphere. (h) The data density, and (i) the ion plasma beta β computed based on SWIA and MAG measurements. Conic fits to the bow shock and MPB are from *Trotignon et al.* [2006].

Using the ranges of values in Table 1, we use the spectra of transport ratios to distinguish the LF wave modes and we plot this identification as a spectrum of wave modes, Figure 1h. In this spectrum, the wave mode is represented by color. We use the following terminology for distinguishing the waves. Alfvén waves refer to both the Alfvén and quasi-parallel slow waves. The fast wave terminology is used for both the quasi-parallel and quasi-perpendicular types. Finally, the slow waves here refer to the quasi-perpendicular type.

For statistical analysis, however, we are mainly interested in the dominant wave modes, i.e., waves with the maximum power. In order to identify the dominant wave modes, we use the magnetic field power spectrum, Figure 1i. We use orbit maps to plot the transport ratios and the wave occurrence ratios corresponding to the dominant waves modes in the Martian upstream region and in the magnetosphere, Figures 2a–2c, 2g, and 3, respectively. We use the Mars-centered Solar Orbital (MSO) coordinate system in these maps that have a spatial grid of 250 km by 250 km (0.06 by 0.06 Mars radii). For the transport ratio maps, in each grid we compute the average transport ratios and color the grid to represent their magnitude. For the wave occurrence ratio maps, in each grid we use a color to represent the number of times a specific wave mode is observed as the dominant wave mode as a fraction of the total number of observations in that grid. To compute these orbit maps, we use data from over 700 MAVEN orbits, from 7 October 2014 to 28 April 2015. The data density is shown in Figure 2h. To yield good statistics, we remove data from orbit maps for the transport ratios and the wave occurrence ratios, if the data density for a given bin is less than 10.

To determine whether the wave occurrence ratios exhibit any variation with the solar wind dynamic pressure, we plot orbit maps of the wave modes with the highest occurrence ratios, i.e., the Alfvén and fast waves in Figure 4. We plot orbit maps for two cases: large and small dynamic pressures. For these orbit maps, we use data from 28 November 2014 to 20 March 2015, where the spacecraft traversed into the upstream region. The solar wind dynamic pressure measured by SWIA in two consecutive orbits is interpolated to obtain the corresponding value when the spacecraft is in the magnetosphere.

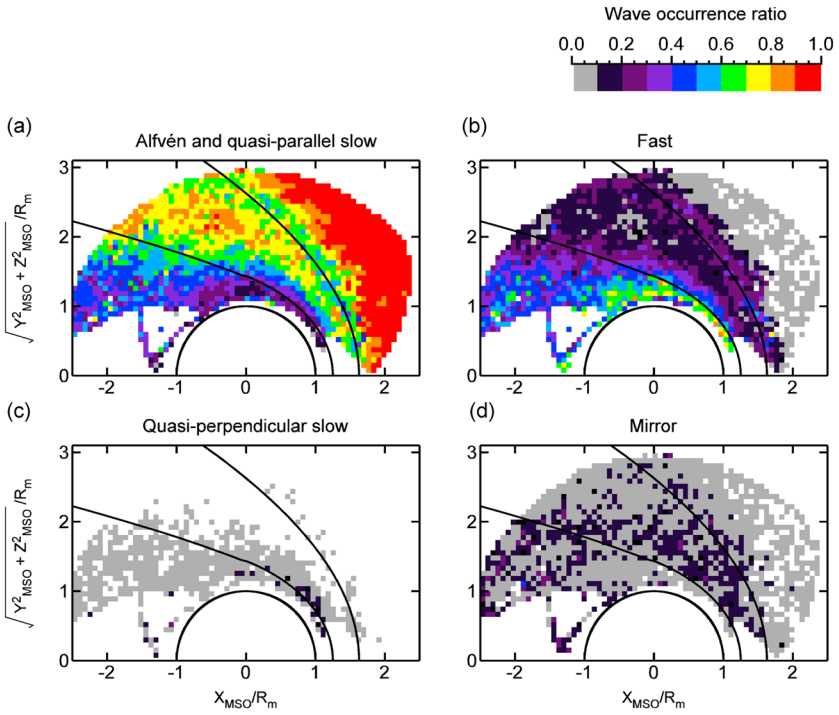

Figure 3. (a–d) Wave occurrence ratios for the four LF wave modes. Alfvén and fast waves have the highest occurrence ratios of the four modes.

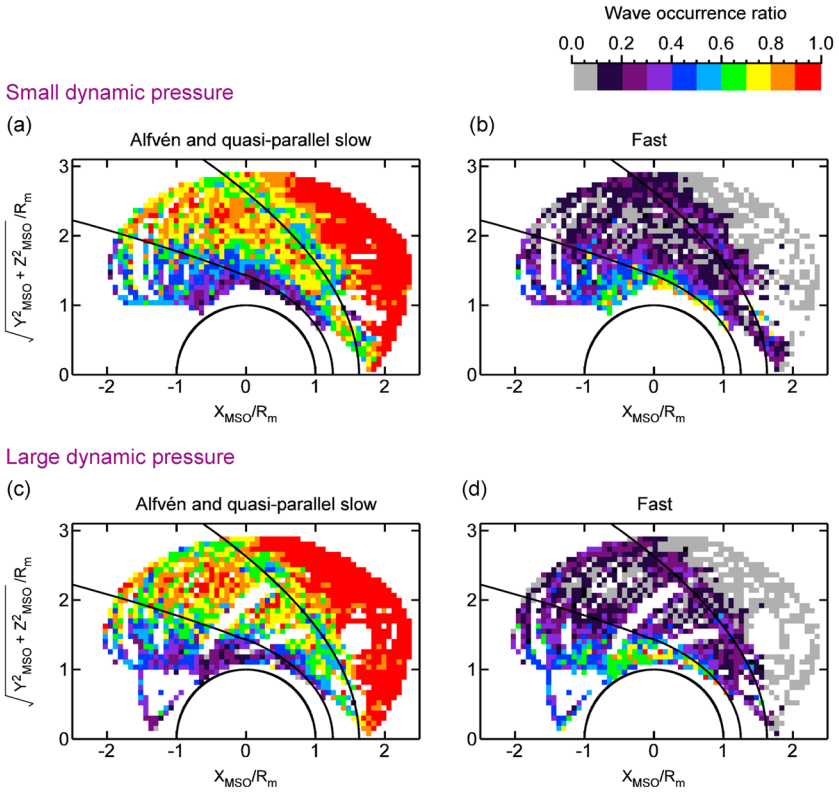

Figure 4. (a–d) Alfvén and fast wave occurrence ratio variability in response to the solar wind dynamic pressure variations. Alfvén waves are enhanced near the bow shock, and the fast wave band is pushed farther inward for the large dynamic pressure case.

4. Caveats

Before discussing the observations, here we note some caveats related to data inside the magnetic pileup boundary (MPB) and steps we have taken to eliminate them. Two of the major issues downstream of the MPB are the SWIA incomplete phase-space coverage and the multi-ion composition of that region. The partial phase-space coverage arises because SWIA only measures ions with energies above 25 eV. SWIA has low count rates corresponding to these instances with partial phase-space coverage and yields low ion moments: typically densities below 0.5 cm^{-3} and velocities below 50 km/s. To ensure that these data do not affect our transport ratios and wave occurrence ratios, we remove these data from our orbit maps, Figures 2a–2c, 2g, 3, and 4.

SWIA does not have mass resolution capability, and consequently, the ion moments it measures in a multi-ion environment such as downstream of the MPB can have significant uncertainties. SWIA assumes hydrogen mass for the ions when computing ion moments; thus, it underestimates the ion density and overestimates the ion velocity [*Halekas et al.*, 2013]. This can lead to significant uncertainties in the computed transport ratios.

To circumvent this issue, we use the STATIC measurements to compute the transport ratios. STATIC has a much wider phase-space coverage (0.1 eV to 30 keV) than SWIA, and it also has mass resolution. We compute transport ratios for STATIC data, starting from time series for ion density and velocity following similar steps used with the SWIA data as described in section 3. The orbit maps for these transport ratios are shown in Figures 2d–2f. Comparison of SWIA and STATIC transport ratios shows good quantitative and qualitative agreement downstream of the MPB, enabling us to be confident in our conclusions. The spacecraft charging affects STATIC low-energy measurements which become significant at very low altitudes. However, this issue does not affect our conclusions because these low altitudes cover only a very small percentage of our observation area.

In addition to these instrument limitations, the wave identification method also has a limitation. The *Song et al.* [1994] method, we use here, was developed to identify waves in a high beta plasma. Downstream of the MPB, magnetic field draping leads to low plasma beta, Figure 2i, and the wave identification method may not be applicable in that region. While we are confident in our measured transport ratios downstream of the MPB, we note that the wave occurrence ratios in that region can have significant uncertainties. Thus, we will not make any definitive conclusions regarding the nature of waves downstream of the MPB.

5. Observations

We will first explore the general trends of the transport ratios in the upstream region and in the magnetosphere. The transverse ratio, Figure 2g, is generally greater than one meaning that the waves are mainly transverse. The waves tend to be more transverse in the upstream region than in the magnetosphere as seen by the higher transverse ratio in the upstream region. The compressional ratio, Figures 2a and 2d, is enhanced when going from the upstream region to deep into the magnetosphere. Generally, the compressional ratio is much less than one in the upstream region, whereas it is much greater than one downstream of the MPB. Since the compressional ratio is a measure of the relative fluctuation strengths of the ion density and the magnetic field, as defined in Table 1, this observation indicates that the upstream is dominated by magnetic field fluctuations, whereas downstream of the MPB is dominated by ion density fluctuations. The phase ratio is the phase difference between the ion density fluctuations and the magnetic field fluctuations parallel to the ambient magnetic field. The phase ratio maps, Figures 2b and 2e, reveal that the parallel magnetic field fluctuations tend to be in phase with the ion density fluctuations upstream, but they tend to be out of phase downstream. Finally, the Doppler ratio maps, Figures 2c and 2f, enable comparison of the relative fluctuations of the ion velocity and the magnetic field. This ratio, is less than one in the upstream region and greater than one downstream of the MPB. Thus, in the upstream region the magnetic field fluctuations exceed the ion velocity fluctuations. The relative magnitudes of these two fluctuations is reversed downstream of the MPB.

We find that the dominant wave modes in the Martian magnetosphere and in the upstream region are the Alfvén and fast waves, Figure 3. This is expected from the inspection of the transport ratios alone, because we found that the transverse ratio is greater than one. Thus, according to Table 1, the wave modes are either the Alfvén or fast waves depending on the value of the compressional ratio.

In particular, we find that the Alfvén waves have the highest occurrence ratio in both the upstream region and in the magnetosheath, Figure 3a, whereas the fast wave occurrence ratio tends to increase when going toward the MPB, Figure 3b. We also find a sudden enhancement of the fast wave occurrence ratio near the bow shock, forming a band-like region. Surprisingly, we find very low occurrence ratios for mirror mode waves, Figure 3d. They are more often found in the dayside magnetosheath. Slow waves have the lowest occurrence ratios, Figure 3c.

Now we will explore the solar wind dynamic pressure dependence for the waves modes, Figure 4. Both Alfvén and fast waves show large occurrence variability near the bow shock. In particular, the Alfvén wave occurrence ratios tend to be higher when the dynamic pressure is high, Figures 4a and 4c. Also, when the dynamic pressure is high, the band of fast waves occurring near the bow shock is pushed farther inward, Figures 4b and 4d.

6. Discussions

This is the first time that the *Song et al.* [1994] technique has been applied for a statistical investigation to identify low-frequency waves over a large spatial scale spanning both the upstream region and in the magnetosphere of any planet in the solar system. The transport ratios, by themselves, allowed us to infer the relative magnitudes and the phase relationships between the ion moment and magnetic field fluctuations.

The observation of the Alfvén waves throughout the magnetosphere, with a gradual decrease of their occurrences as one ventures deeper into the magnetosphere, is indicative of the penetration of the upstream Alfvén waves. With the use of Mars Express, *Lundin et al.* [2011] found that the low-frequency wave intensity enhances with increasing solar wind dynamic pressure, and they also found that there is penetration of magnetosheath waves into low altitudes. Our results are indicative of a more extensive penetration, the upstream Alfvén waves seem to penetrate all the way toward the MPB and possibly even deeper into the MPR. However, we do not see a significant enhancement of the Alfvén wave occurrence ratios inside the magnetosheath when the dynamic pressure is high. Thus, it is an open question as to what causes the Mars Express observations of the wave intensity enhancement. A likely explanation is an enhancement of the Alfvén wave power for large dynamic pressure but not necessarily their occurrence ratios. This needs to be investigated further with the inclusion of MAVEN data from an extended mission.

With a case study of the MGS data, *Bertucci et al.* [2004] observed fast waves on the downstream side of the MPB. We observe a high occurrence ratio for the fast waves near the upstream side and downstream of the MPB. However, as discussed in section 4, the possible uncertainties associated with the wave occurrence ratios downstream of the MPB precludes us to make any definitive conclusions about the nature of the waves in that region. *Glassmeier and Espley* [2006] suggested that the MPB can act as a cavity that sustains global oscillations in the form of fast waves. A possible source for these waves is the Kelvin-Helmholtz (KH) instability. While we are yet to find definitive evidence for the KH instability operating at Mars, this instability is expected for unmagnetized planets [*Amerstorfer et al.*, 2007]. Investigation of the Earth magnetosphere has shown that observation of the fast waves in the magnetosheath could be an indication of the KH instability operating in the magnetopause [*Borisov and Fränz*, 2011].

The sudden increase of the fast wave occurrence ratio near the bow shock is suggestive of the excitation of these waves due to bow shock phenomena such as reflection of ions and leakage of magnetosheath plasma into the upstream region. However, to be conclusive, we need to investigate more into the variability of these waves in response to upstream conditions such as the interplanetary magnetic field direction. The observed variability of the fast waves and the Alfvén waves near the bow shock with the upstream dynamic pressure can be associated with the movement of the bow shock.

Bertucci et al. [2004] observed mirror mode waves on the upstream side, and *Espley et al.* [2004] suggested that mirror mode wave are the dominant wave modes in the dayside magnetosheath. We find that mirror wave occurrence ratio is lower than both the Alfvén and fast waves. However, it has a relatively high occurrence ratio in the dayside magnetosheath.

While we find that the slow waves have the lowest occurrence ratio of the four wave modes, it is relatively high in the magnetosheath near the MPB and highest near the subsolar point. Slow mode waves were found near the Earth magnetopause [*Song et al.*, 1992, 1990], and MHD simulations have indicated that these waves arise as a consequence of interaction of the upstream waves with the bow shock [*Yan and Lee*, 1994].

7. Summary and Conclusions

We used the MAVEN SWIA, STATIC, and MAG measurements for characterizing the low-frequency waves at Mars in the upstream region and in the magnetosphere. Using transport ratios, we identified the dominant wave modes and characterized their occurrence ratios. We also observed wave occurrence variability with the upstream dynamic pressure which indicates that the upstream drivers play an important role for the waves.

Acknowledgments
This work was supported by NASA and was partially supported by the CNES. MAVEN data are publicly available through the Planetary Data System.

The Editor thanks Laila Andersson and an anonymous reviewer for their assistance in evaluating this paper.

References

Amerstorfer, U. V., N. V. Erkaev, D. Langmayr, and H. K. Biernat (2007), On Kelvin-Helmholtz instability due to the solar wind interaction with unmagnetized planets, *Planet. Space Sci.*, *55*, 1811–1816.

Bertucci, C., C. Mazelle, D. H. Crider, D. L. Mitchell, K. Sauer, M. H. Acuña, J. E. P. Connerney, R. P. Lin, N. F. Ness, and D. Winterhalter (2004), MAG/ER observations at the magnetic pileup boundary of Mars: Draping enhancement and low frequency waves, *Adv. Space Res.*, *33*, 1938–1944.

Bertucci, C., N. Romanelli, J. Y. Chaufray, D. Gomez, C. Mazelle, M. Delva, R. Modolo, F. González-Galindo, and D. A. Brain (2013), Temporal variability of waves at the proton cyclotron frequency upstream from Mars: Implications for Mars distant hydrogen exosphere, *Geophys. Res. Lett.*, *40*, 3809–3813, doi:10.1002/grl.50709.

Blanco-Cano, X., and S. J. Schwartz (1997), Identification of low-frequency kinetic wave modes in the Earth's ion foreshock, *Ann. Geophys.*, *15*, 273–288.

Borisov, N., and M. Fränz (2011), Excitation of low frequency oscillations in a planetary magnetosheath by supersonic shear flow, *Nonlinear Processes Geophys.*, *18*, 209–221.

Brain, D. A., F. Bagenal, M. H. Acuña, J. E. P. Connerney, D. H. Crider, C. Mazelle, D. L. Mitchell, and N. F. Ness (2002), Observations of low-frequency electromagnetic plasma waves upstream from the Martian shock, *J. Geophys. Res.*, *107*(A6), 1076, doi:10.1029/2000JA000416.

Connerney, J. E. P., J. Espley, P. Lawton, S. Murphy, J. Odom, R. Oliversen, and D. Sheppard (2014), The MAVEN magnetic field investigation, *Space Sci. Rev.*, doi:10.1007/s11214-015-0169-4.

Denton, R. E., S. P. Gary, X. Li, B. J. Anderson, J. W. LaBelle, and M. Lessard (1995), Low-frequency fluctuations in the magnetosheath near the magnetopause, *J. Geophys. Res.*, *100*, 5665–5679.

Ergun, R. E., L. Andersson, W. K. Peterson, D. Brain, G. T. Delory, D. L. Mitchell, R. P. Lin, and A. W. Yau (2006), Role of plasma waves in Mars' atmospheric loss, *Geophys. Res. Lett.*, *33*, L14103, doi:10.1029/2006GL025785.

Espley, J. R., P. A. Cloutier, D. A. Brain, D. H. Crider, and M. H. Acuña (2004), Observations of low-frequency magnetic oscillations in the Martian magnetosheath, magnetic pileup region, and tail, *J. Geophys. Res.*, *109*, A07213, doi:10.1029/2003JA010193.

Espley, J. R. (2005), Low frequency plasma waves at Mars, PhD. thesis, Dept. of Phys. and Astron., Rice Univ., Houston, Texas, USA.

Gary, S. P. (1991), Electromagnetic ion/ion instabilities and their consequence in space plasmas: A review, *Space Sci. Rev.*, *56*, 373–415.

Gary, S. P. (1993), *Theory of Space Plasma Microinstabilities*, Cambridge Univ. Press, Cambridge, U. K.

Glassmeier, K.-H., and J. Espley (2006), ULF waves in planetary magnetospheres, in *Magnetospheric ULF Waves: Synthesis and New Directions*, edited by K. Takahashi et al., AGU, Washington, D. C.

Gurnett, D. A., D. D. Morgan, F. Duru, F. Akalin, J. D. Winningham, R. A. Frahm, E. Dubinin, and S. Barabash (2010), Large density fluctuations in the Martian ionosphere as observed by the Mars Express radar sounder, *Icarus*, *206*, 83–94.

Gunell, H., et al. (2008), Shear driven waves in the induced magnetosphere of Mars, *Plasma Phys. Controlled Fusion*, *50*, 074018.

Halekas, J. S., E. R. Taylor, G. Dalton, G. Johnson, D. W. Curtis, J. P. McFadden, D. L. Mitchell, R. P. Lin, and B. M. Jakosky (2013), The solar wind ion analyzer for MAVEN, *Space Sci. Rev.*, doi:10.1007/s11214-013-0029-z.

Hubert, D., C. Lacombe, C. C. Harvey, M. Moncuquet, C. T. Russell, and M. F. Thomsen (1998), Nature, properties, and origin of low-frequency waves from an oblique shock to the inner magnetosheath, *J. Geophys. Res.*, *103*, 26783–26798.

Lundin, R., S. Barabash, E. Dubinin, D. Winningham, and M. Yamauchi (2011), Low-altitude acceleration of ionospheric ions at Mars, *Geophys. Res. Lett.*, *38*, L08108, doi:10.1029/2011GL047064.

Mazelle, C., et al. (2004), Bow shock and upstream phenomena at Mars, *Space Sci. Rev.*, *111*, 115–181.

McFadden, J. P., et al. (2014), The MAVEN Suprathermal and Thermal Ion Composition (STATIC) instrument, *Space Sci. Rev.*

Romanelli, N., C. Bertucci, D. Gómez, C. Mazelle, and M. Delva (2013), Proton cyclotron waves upstream from Mars: Observations from Mars Global Surveyor, *Planet. Space Sci.*, *76*, 1–9.

Russell, C. T., J. G. Luhmann, K. Schwingenschuh, W. Riedler, and Y. Yeroshenko (1990), Upstream waves at Mars—Phobos observations, *Geophys. Res. Lett.*, *17*, 897–900.

Russell, C. T., J. G. Luhmann, K. Schwingenschuh, W. Riedler, and Y. Yeroshenko (1992), Upstream waves at Mars, *Adv. Space Res.*, *12*, 251–254.

Schwartz, S. J., D. Burgess, and J. J. Moses (1996), Low-frequency waves in the Earth's magnetosheath: Present status, *Ann. Geophys.*, *14*, 1134–1150.

Song, P., C. T. Russell, J. T. Gosling, M. Thomsen, and R. C. Elphic (1990), Observation of the density profile in the magnetosheath near the stagnation streamline, *Geophys. Res. Lett.*, *17*, 2035–2038.

Song, P., C. T. Russell, and M. F. Thomsen (1992), Slow mode transition in the frontside magnetosheath, *J. Geophys. Res.*, *97*, 8295–8305.

Song, P., C. T. Russell, and S. P. Gary (1994), Identification of low-frequency fluctuations in the terrestrial magnetosheath, *J. Geophys. Res.*, *99*, 6011–6025.

Trotignon, J. G., C. Mazelle, C. Bertucci, and M. H. Acuña (2006), Martian shock and magnetic pile-up boundary positions and shapes determined from the Phobos 2 and Mars Global Surveyor data sets, *Planet. Space Sci.*, *54*, 357–369.

Wei, H. Y., and C. T. Russell (2006), Proton cyclotron waves at Mars: Exosphere structure and evidence for a fast neutral disk, *Geophys. Res. Lett.*, *33*, L23103, doi:10.1029/2006GL026244.

Winningham, J. D., et al. (2006), Electron oscillations in the induced Martian magnetosphere, *Icarus*, *182*, 360–370.

Yan, M., and L. C. Lee (1994), Generation of slow-mode waves in front of the dayside magnetopause, *Geophys. Res. Lett.*, *21*, 629–632.